A Novel Method for Measuring Radiated Common Mode Current of Isolated Power Converters

Qingbin CHEN, Qinwen YANG, Jianxin SHI, and Shaohui XU

***Abstract*—At radiated frequencies, common mode (CM) current is the dominant radiation source for isolated power converters with long cables attached. Based on the existing radiation noise model, this paper proposes a novel method to measure CM current using a current transformer (CT), which has a higher transfer impedance and can measure the radiation noise in a broader frequency range than the traditional high-frequency (HF) clamp-on current probe. According to the established CT model, the corresponding design methods are proposed to improve the bandwidth and transfer impedance and the final CT that meets the requirements is determined after comparing different methods. The practicability and effectiveness of the designed CT are verified by comparing the measured CM current with the final anechoic chamber measurement results.**

***Index Terms*—Bandwidth and transfer impedance, common mode (CM) current, current transformer (CT), high-frequency clamp-on current probe, isolated power converters, radiated EMI.**

I. Introduction

With the advancement in power converters characterized by high power density and increased frequency, coupled with the integration of wide bandgap semiconductor devices, electromagnetic interference (EMI) has emerged as a progressively critical issue. The conducted EMI has been investigated in many papers [1]–[6]. However, only some papers address radiated EMI for power electronics applications. Converters must comply with international regulations and standards, such as EN55022 and CISPR 22, before they are allowed to commercialize. In industrial contexts, the escalating severity of radiated EMI from power converters poses significant challenges in meeting these standards, thereby necessitating a deeper investigation into radiated EMI phenomena.

In the radiating frequency band for isolated power converters connected to long cables, the common-mode (CM) current is the main source of noise, while the differential-mode (DM) current loop is small due to the small size of the converter [7]. Yao *et al*. [8] analyzed a radiation model based on a flyback converter. Their modeling of flyback converters can be extended to the general radiation model of isolated power converters with long input-output cables. Fig. 1 depicts the flowing path of the CM current. In AC input applications, the isolated power converter generally consists of an input rectifier bridge, primary circuit, transformer, secondary side rectifier and filter. Existing studies show that winding terminals become high du/dt nodes due to switches on and off [9]. CM current can flow from the primary side to the secondary side through parasitic parameters between transformers and finally flow back to the noise source through antennas formed by input and output cables. Therefore, the transformer is the only way for CM current. According to the formation mechanism of radiated EMI and the flowing path of CM current, many corresponding solutions have been put forward in relevant papers [8], [10]–[12].

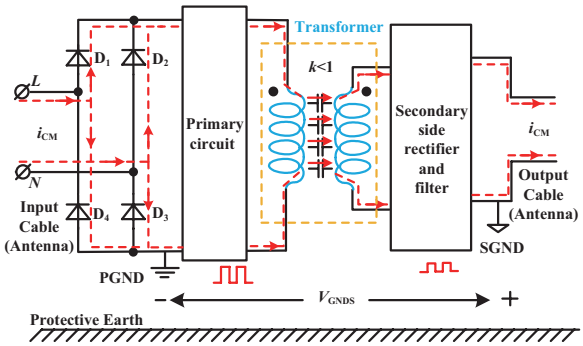

Fig. 1. The flowing path of CM current for isolated power converters

Addressing radiated EMI hinges on curbing CM current, achievable through three primary strategies: switching noise reduction, EMI filter design, and transformer optimization. The first method usually results in a switching speed decrease and switching loss increase, so it is not preferred [10]. EMI filter design includes the design of CM choke and Y capacitor. High-frequency lossy magnetic material-based CM chokes are designed in paper [8]–[11]. The use of the designed CM chokes makes a substantial reduction in radiated EMI. According to the radiation model of the flyback converter in the paper [8], the Y capacitor is connected in parallel at both ends of the antenna. Due to the lower impedance in the radiated frequency band than the antenna impedance, the Y capacitor can bypass most of the CM current to reduce radiated EMI significantly. The third approach of transformer design is to decrease the transformation

Manuscript received August 4, 2024; revised September 13, 2024; accepted September 26, 2024. Date of publication December 30, 2024; date of current version October 18, 2024. No funding was received to assist with the preparation of this manuscript. *(Corresponding author: Qingbin Chen.)*

Q. Chen, Q. Yang, and S. Xu are with the College of Electrical Engineering and Automation, Fuzhou University, Fuzhou, Fujian 350108, China (e-mail: cqb@fzu.edu.cn; 466177245@qq.com; 673544196@qq.com).

J. Shi is with Future Technology Co., Ltd., Hangzhou, Zhejiang 310000, China (e-mail: 2541784392@qq.com).

Digital Object Identifier 10.24295/CPSSTPEA.2024.00021

from differential mode noise to common mode noise [12].

When a radiated common-mode current flows through an antenna, it emits electromagnetic waves into space. The results measured in the anechoic chamber can be predicted by establishing the relationship between the CM current and the electromagnetic field. Padungtin *et al*. [13] demonstrated the relationship between the radiated CM current and the radiated electric field intensity based on a simple short dipole antenna. As the antenna structure was not considered, and the CM current was measured in the middle part of the cable, the final predicted result was quite different from the actual anaphora measurement result. Zhang *et al*. [14] proposed a general radiated model for isolated power converters with long cables attached. The model fully considers the influence of the antenna structure on the CM current and predicts the final electric field strength by measuring the common-mode current on the cable with EZ17. Nevertheless, the limited transfer impedance and frequency range of EZ17 influence the accuracy of these measurements.

This paper proposes a method for measuring the radiated common mode current. Compared with the measurement method using EZ17, it has higher bandwidth and transfer impedance, so it can measure a broader range and a smaller value of radiated noise. Through the measured radiation noise, the final EMI measured in the anechoic chamber can be predicted, thus saving time and energy. This paper is mainly divided into the following parts. In Section II, the existing radiation noise model is reviewed. The model establishes the relationship between the radiation common mode current and the maximum electric field strength. In Section III, the CT is modeled to measure the common mode current. In Section IV, the design of CT is discussed by comparing several methods. The Section V contrasts CT measurement results with anechoic chamber data, using the established radiation model to predict the final electric field intensity. Experimental validation is given in Section VI. The paper concludes with a summary in Section VII.

II. Radiation Noise Model and Traditional CM Current Measurement Method

Owing to the power converter's high power density and the development of high switching frequency, the volume of the converter is significantly reduced. However, long input power and output lines are always needed to connect to other modules in many applications. When the cable length exceeds 1/4 wavelength, input and output cables are considered as an antenna. At the same time, the transformer is usually used in isolated power converters to separate the input and output. When there is a voltage difference between the primary and secondary, this voltage difference will act on both ends of the antenna, making the antenna flow through the CM current and finally forming radiated EMI noise in space. Therefore, it is generally believed that CM current is the main noise source of radiation, and the radiation noise generated by differential mode current can be ignored. The radiation schematic of the isolated power converter with long cables is shown in Fig. 2.

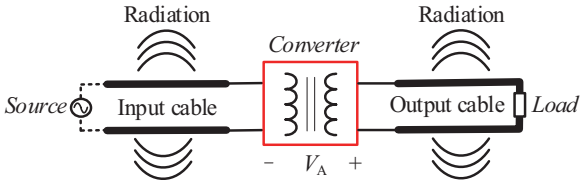

Fig. 2. General radiation noise model of isolated power converters.

Relevant standards stipulate that the measurement of radiated EMI must be carried out in an anechoic room [15], and a receiving antenna is required to receive the electromagnetic noise radiated by the DUT, so the electric field strength in the space is measured in the anechoic room. The common mode current generates this electric field strength. The radiated EMI can be predicted by establishing the relationship between the common mode current and the electric field strength. In the paper [16], based on the electromagnetic field theory and antenna theory, the relationship between the CM current and the electric field strength under arbitrary antenna structures is derived, as shown in (1) and (2).

$$E_{\max} = \sqrt{\frac{\eta G}{4\pi r^2}} \times \left|\dot{I}_A\right| \times \sqrt{R_A} \tag{1}$$

$$G = eD \tag{2}$$

In the formula, E_{max} is the maximum electric field intensity in the space, which is the value measured in the chamber; η is the characteristic impedance in the space, which is 120π Ω; G is the antenna gain, which depends on the structure of the antenna and is a frequency that changes. Parameters r represents the distance between the antenna and the measurement point, which is 3 m or 10 m according to the standard; I_A is the CM current flowing through the antenna; R_A represents the total resistance of the antenna, which also includes the antenna loss power equivalent resistance R_r and the antenna radiated power equivalent resistance R_l. Parameters e is the radiation efficiency of the antenna, which is equal to R_r/R_A.

According to the measurement standard of radiated EMI, the placement of the input power line and the output line is fixed, so the structural parameters of the antenna cannot be changed. G and R_A in the formula are determined, and η and r are also fixed, so the only factor affecting the electric field strength is the CM current I_A. Accurate measurement of CM current becomes a top priority for predicting radiated EMI.

CM current can be measured using a high-frequency current probe connected to the spectrum analyzer. It is worth noting that the current probe must be placed less than 1/4 wavelength, generally placed close to the EUT outlet [17]. The setup for its experimental measurements is shown in Fig. 3.

To measure the common mode current in the radiation frequency band (30 MHz~1 GHz), the frequency range covered by the current probe must meet the entire radiation frequency band. However, the frequency band of many current probes on the market is far less than 1 GHz, such as the EZ17 model 02

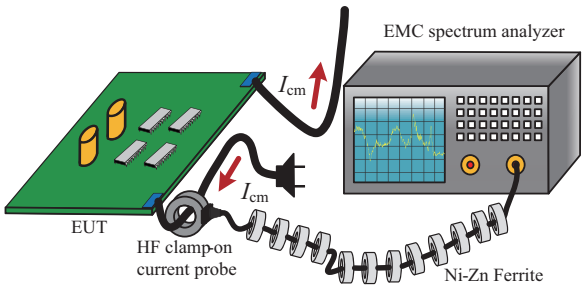

Fig. 3. CM current test setup diagram (EZ-17).

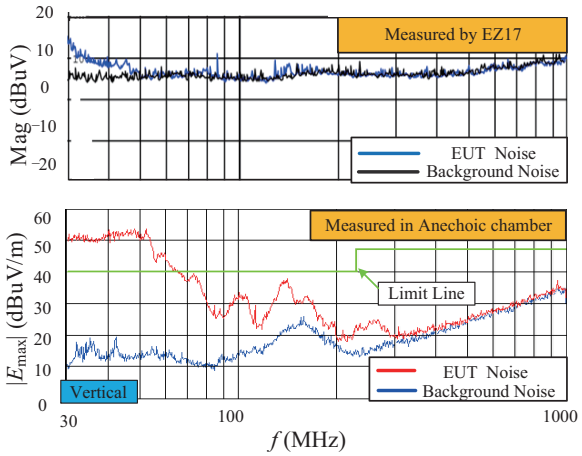

Fig. 4. Comparison of EZ17 measurement results and anechoic chamber measurement results.

of Rohde & Schwarz Company, which covers a frequency that is only 20 Hz~100 MHz, far from meeting the expectations.

Because of its small transfer impedance, when the noise source signal is small, the spectrum reflected on the receiver will be covered by the noise floor, so the magnitude of the common mode current cannot be accurately obtained. The actual measured common mode current with EZ17 and the noise spectrum of the anechoic room test are shown in Fig. 4. It can be seen that the common mode current noise is almost covered by the noise floor in the 46 MHz~1 GHz frequency band, and there is still noise in this frequency band in the anechoic chamber. Therefore, the CM current measured by the EZ17 cannot predict the final anechoic chamber test results.

III. Analysis and Modeling of CT

According to the analysis in the first section, the CM current mainly generates radiated noise, and there is a certain relationship between the maximum electric field strength and the CM current. Therefore, if the CM current can be accurately measured, the radiated electromagnetic interference can be predicted. Most laboratories are equipped with high-frequency current probes to measure the noise current, but the range they cover is far from the radiation frequency range. Due to their small transfer impedance, the spectrum displayed on the EMC spectrometer will be covered by the ground noise, so a current probe with a higher transfer impedance and higher bandwidth

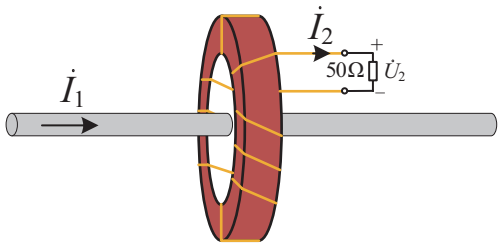

Fig. 5. Structure diagram of CT.

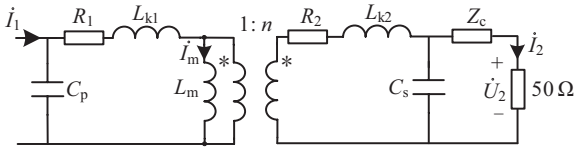

Fig. 6. The equivalent circuit of CT.

is supposed to be designed.

Based on the annular structure of the high-frequency current probe, the annular magnetic core is selected as the research object, and its structure diagram is shown in Fig. 5. The designed CT is similar to a transformer with a turn ratio of 1: n. Its primary winding is the input or output cable connected to the power converter. It has only 1 turn through the magnetic ring, and I_1 is the CM current flowing on the cable to be measured; the secondary winding is an n-turn coil, and the outlet end of the n-turn coil is connected to the internal 50 Ω resistor of the EMC spectrum analyzer through a coaxial cable. When the CM current I_1 flows on the input cable or the output cable, the CM current will establish a changing magnetic field in the magnetic ring, and the changing magnetic field will induce a voltage on the secondary winding. When the load is 50 Ω, the induced voltage is the final voltage value displayed on the spectrum analyzer.

A. Modeling of CT

Based on the transformer structure in Fig. 5, it can be equivalent to the transformer model in Fig. 6. Among them, the leakage inductances L_{k1} and L_{k2} represent the equivalent inductance of the leakage flux on the primary side and the secondary side; the magnetizing inductance L_m represents the equivalent inductance of the main magnetic flux established in the magnetic ring; C_p and C_s represent the parasitic capacitance of the primary windings and the secondary winding respectively; R_1 and R_2 represent the parasitic resistance of the primary and secondary windings; Z_c represents the impedance of the coaxial cable of the receiver; the 50 Ω load is the internal sampling resistor.

B. Determination of Secondary Turns

To make the designed CT have a higher transfer impedance, which means to make the ratio of U_2 to I_1 in Fig. 6, and obtain a larger U_2 under the same common mode current, the number of turns of the secondary winding needs to be designed.

a) Simplified model

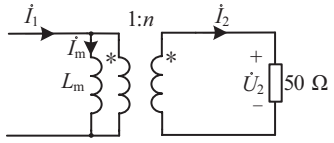

Fig. 7. The simplified circuit of CT.

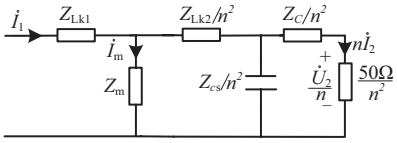

Fig. 8. The specific circuit of CT.

For the convenience of analysis, we assume the ratio of the turns of the primary and secondary sides remains 1:n, and ignore the influence of related parasitic parameters (discussed below). The simplified circuit diagram is shown in Fig. 7.

Therefore, the ratio of the current between the primary and secondary sides can be established:

$$\frac{\dot{I}_2}{\dot{I}_1}=\frac{Z_m}{\frac{50}{n^2}+Z_m}\cdot\frac{1}{n}=\frac{1}{\frac{50}{n^2\cdot Z_m}+1}\cdot\frac{1}{n} \tag{3}$$

where Z_m is the impedance of the magnetizing inductance. Since Z_m is much larger than 50 Ω in the radiation frequency band, (5) can be derived from (3):

$$\left|\frac{50}{n^2\cdot Z_m}\right|<<1 \tag{4}$$

$$\begin{cases}\dfrac{\dot{I}_2}{\dot{I}_1}\approx\dfrac{1}{n}\\ Z_t=\dfrac{\dot{U}_2}{\dot{I}_1}=\dfrac{50\dot{I}_2}{\dot{I}_1}=\dfrac{50}{n}\end{cases} \tag{5}$$

To make the measured noise greater than the background noise, U_2 should be greater than the background noise. The larger I_2 and Z_t are, the easier it is to achieve the effect. So the smaller the value of n, the better the effect. Choose n to be 1, so the secondary side is also one turn, ensuring that Z_t is the maximum.

b) Specific model

When the influence of parasitic parameters cannot be ignored, the equivalent circuit is shown in Fig. 8. Since the number of primary-side turns always remains one turn, its capacitance C_p can usually be ignored. Therefore, the equivalent circuit of converting the secondary side to the primary side is as in Fig. 8.

C. Influence of Magnetic Ring Characteristics on Transfer Impedance

The transfer impedance is not only related to the number of turns but also to the characteristics of the magnetic ring itself. The following formula can explain the influence of the magnetic ring on the transfer impedance.

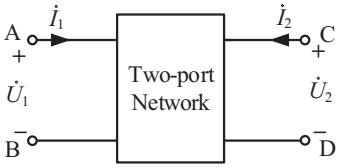

Fig. 9. Schematic diagram of the two-port test.

When n is equal to 1:

$$\begin{cases}Z_t=\dfrac{\dot{U}_2}{\dot{I}_1}\\ \dot{U}_2=\dfrac{j\omega L_m}{R+j\omega L_m}\cdot\dot{I}_1\cdot R\end{cases} \tag{6}$$

So:

$$Z_t=\frac{1}{\frac{1}{j\omega L_m}+\frac{1}{R}} \tag{7}$$

where R=50 Ω, Z_t is proportional to L_m, and if you want to increase Z_t, you can increase L_m. For a ring core, the inductance satisfies the following relation:

$$L_m\propto\frac{\mu_e\cdot A_e}{l_e} \tag{8}$$

That is, the magnetizing inductance is proportional to the relative permeability and the cross-sectional area of the magnetic circuit, and inversely proportional to the magnetic circuit length. Therefore, to increase the magnetizing inductance L_m, the magnetic ring with larger permeability in the radiation band can be selected, or the cross-sectional area A_e can be increased or the length l_e can be decreased.

IV. Optimal Design of CT

According to the modeling of the converter in Section III, to increase the transfer impedance of CT, the number of turns of the secondary side must be set as one turn, and increasing the inductance of excitation can also increase the transfer impedance. Therefore, the following CT design aims to increase the inductance of excitation.

A. CT Design Evaluation Index

The current converter is similar to a two-port network, and the two-port parameters can be measured by the network analyzer, as shown in Fig. 9, and the transfer impedance Z_t can be calculated, and the calculation is deduced as follows:

$$\begin{cases}\dot{I}_1=\dot{U}_1\times Y_{11}+\dot{U}_2\times Y_{12}\\ \dot{I}_2=\dot{U}_1\times Y_{21}+\dot{U}_2\times Y_{22}\\ \dot{I}_2=-\dfrac{\dot{U}_2}{50}\end{cases} \tag{9}$$

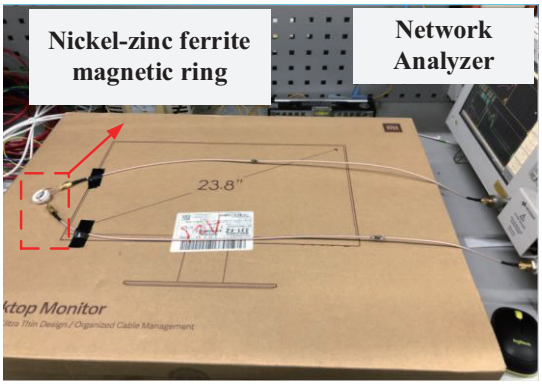

Fig. 10. The two-port measurement diagram of nickel-zinc ferrite.

According to (9), it can be obtained that the transfer impedance of CT is:

$$Z_t = \frac{\dot{U}_2}{\dot{I}_1} = \frac{1}{\frac{Y_{11}}{Y_{21}}(-Y_{22} - \frac{1}{50}) + Y_{12}} \tag{10}$$

Therefore, for CTs of different designs, it is only necessary to compare the transfer impedances converted from the port characteristics. The measurement setup is as shown in Fig. 10.

B. CT Design Method

a) Selection of core material

To ensure that the current transformer (CT) retains its transformer characteristics within the radiation frequency band, it is imperative to select a core material that maintains a certain level of permeability in this frequency range.

The selection of the magnetic core material is a selection of the equivalent magnetic permeability of the magnetic core material. The μ_e should not exhibit drastic changes with frequency and must sustain a reasonable level of magnetic permeability at higher frequencies. Given that the effective frequency range of the equivalent magnetic permeability for manganese-zinc ferrite materials is approximately below 5 MHz, and considering that its permeability rapidly diminishes above 5 MHz, manganese-zinc ferrites fall short of the requirements for the radiation frequency band and are thus initially excluded from consideration. Consequently, the focus shifts to comparing the differences between nickel-zinc ferrite and magnetic powder cores, as these materials are more likely to meet the necessary criteria for the radiation frequency band.

The two cores used for comparison are nickel-zinc ferrite and magnetic powder core S026 of FeSiAl, both of which have the same size specifications, TX22x14x6.4(TX outer diameter × inner diameter × height). According to the curve of permeability change with frequency provided in Fig. 11, it can be found that the permeability of two types of magnetic cores decreases with the increase of frequency. Since the maximum frequency of the curve provided by the magnetic powder core manufacturer is only up to 10 MHz, the permeability of the two radiation bands cannot be compared. Therefore, the transfer

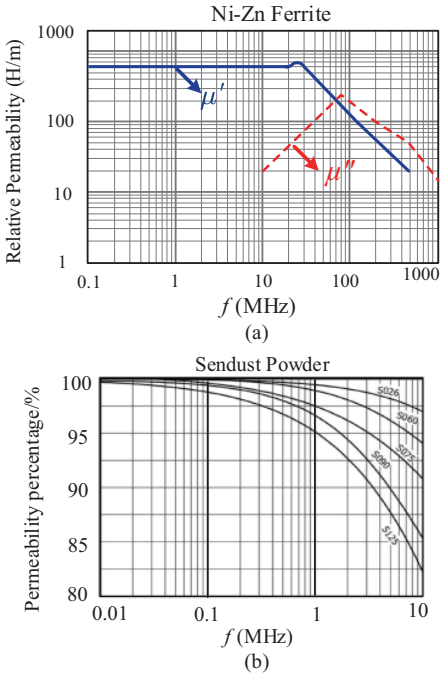

Fig. 11. Magnetic permeability versus frequency curve. (a) Ni-Zn ferrite. (b) Sendust Powder.

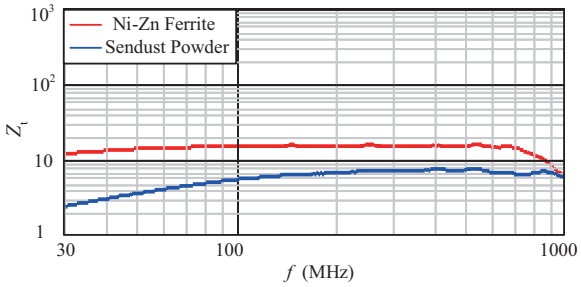

Fig. 12. Transfer impedance curves of Ni-Zn ferrite and Sendust powder.

impedance Z_t was used for evaluation. The measured Z_t curves of the two are shown in Fig. 12.

The graphical analysis reveals that the transfer impedance characteristics of nickel-zinc ferrite exhibit a more stable profile compared to those of the ferrosilicon Al magnetic powder core within the 30 MHz to 700 MHz frequency band. Notably, a significant drop in transfer impedance for nickel-zinc ferrite is observed only beyond 700 MHz. Furthermore, the magnitude of the transfer impedance of nickel-zinc ferrite is considerably higher, particularly in the 30 MHz to 100 MHz range.

b) Magnetic core size design

According to the comparison of Z_t in Fig. 12, Ni-Zn ferrite is more suitable for CT design than powder core, so this magnetic material is used in the following discussion.

① *Increase the number of magnetic rings*

As shown in Fig. 13(a), the model and size of magnetic rings are TX22x14x6.4. After the network analyzer measures the S parameter, its transfer impedance can be calculated. The result is shown in Fig. 13(b). With the increased number of magnetic rings and the CT transfer impedance Z_t increases significantly

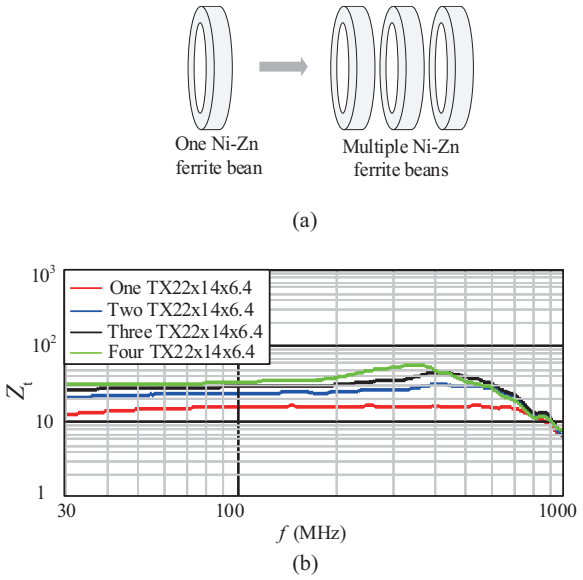

Fig. 13. (a) Increase the number of magnetic rings. (b) Z_t comparison of different numbers of magnetic rings.

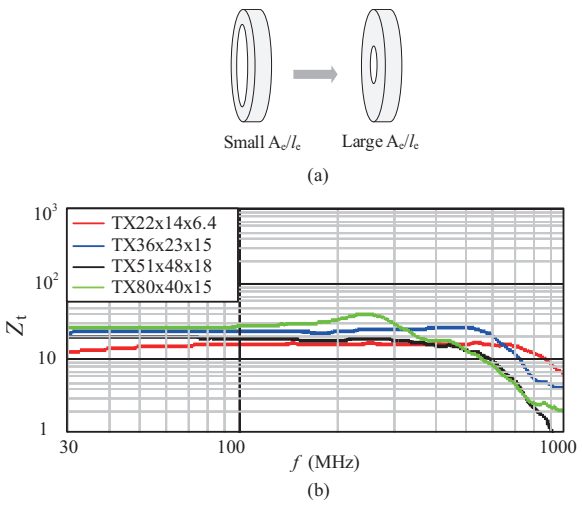

Fig. 14. (a) Choose rings with different cross-sectional areas and magnetic circuit sizes. (b) Z_t comparison of different ratios of cross-sectional area to the magnetic circuit.

at low frequency. Still, in the frequency band above 700 MHz, the change of the transfer impedance is not obvious, and with the frequency change, the change of the transfer impedance of multiple magnetic rings is more drastic than that of a single magnetic ring.

② *Select a magnetic ring with a larger ratio of cross-sectional area to the magnetic circuit*

As shown in Fig. 14(a), the model sizes are respectively TX22x14x6.4, TX36x23x15, TX51x48x18 and TX80x40x15. The transfer impedance comparison is shown in Fig. 14(b). With different models, the transfer impedance below 200 MHz increases significantly, and the change of transfer impedance is more stable, which meets the expectation. However, when the transfer impedance is above 200 MHz, the change is more drastic and the transfer impedance becomes smaller.

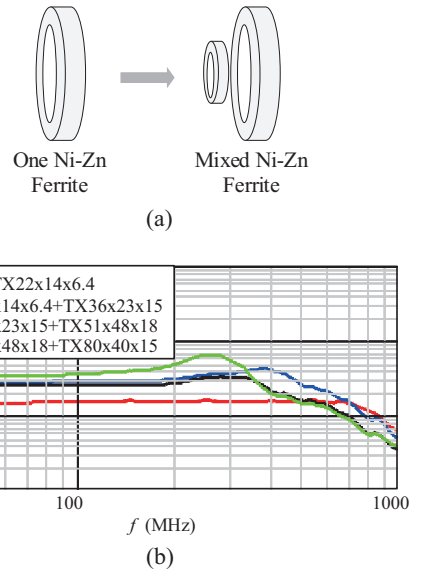

Fig. 15. (a) Mixing of different sizes of magnetic rings. (b) Z_t comparison of Multiple magnetic rings superimposed.

③ *Mix magnetic rings of different-sized*

The analysis of Fig. 15 indicates that if the noise below 200 MHz is analyzed, it is better to measure the noise obtained by using a large-size magnetic ring. When analyzing noise in higher frequency bands, it is better to use a single magnetic ring because its transfer characteristics are more stable and more suitable as a current transformer for evaluating radiated EMI.

Fig. 16 shows the design of CT and the sequence of its optimization.

V. The Calibration of CT

The unknown EMI current flowing in a cable can be calculated if current probe transfer impedance Z_t is known at a given frequency(all in decibels)

$$I = V - Z_t \tag{11}$$

where,

I = the unknown EMI current flowing in a cable in dBμA.

V= the output voltage of the current probe measured in dBμV with a spectrum analyzer.

Z_t = the transfer impedance of the current probe in dBΩ.

Based on the above analysis and optimization design, within the full frequency band (30 MHz~1 GHz), a current transformer made from the TX22x14x6.4 single magnetic ring of nickel-zinc ferrite was selected. Its transfer impedance is more stable and the bandwidth is 800 MHz. At this frequency point, the transfer impedance is attenuated to 0.5 times of the original. The transfer impedance of the selected CT is shown in Fig. 17.

Compared with other self-made probes in the literatures [18], [19] and the commercial probe EZ-17, it has a larger transfer impedance, is flatter, and has lower attenuation in the high-frequency band. Moreover, the bandwidth reaches 800 MHz. Therefore, for the common-mode current with a smaller amplitude, the designed CT can measure the magnitude and varia-

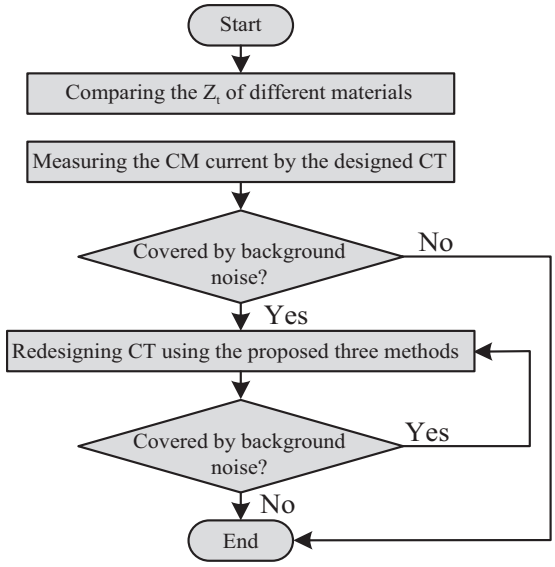

Fig. 16. The design flow chart of CT.

TABLE I
THE MAIN ELECTRICAL PARAMETERS OF THE PROTOTYPE

Input voltage V_{in}	Output voltage V_{out}	Output power P_{out}	Switching frequency f
AC 220 V/50 Hz	DC 12 V	60 W	90 kHz

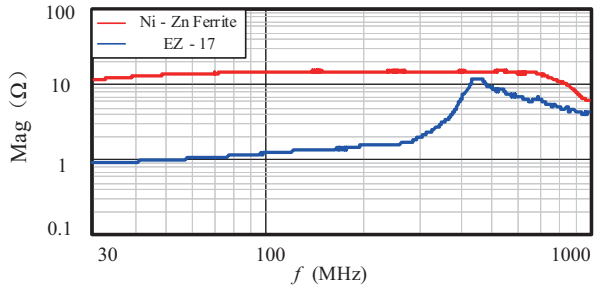

Fig. 17. Transfer impedance(Z_t) for selected CT.

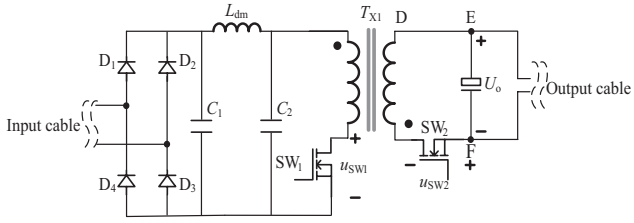

Fig. 18. Flyback power adapter circuit schematic.

tion trend of the common-mode current better than EZ-17.

VI. EXPERIMENTAL VALIDATION

The prototype used in the experiment is the flyback power supply with Y capacitors and filters.

The main parameters are shown in Table I, the main circuit structure is shown in Fig. 18, and the physical diagram is shown in Fig. 19.

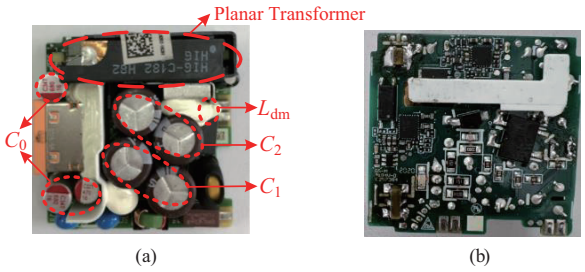

Fig. 19. Physical diagram of flyback power adapter. (a) Front side. (b) Back side.

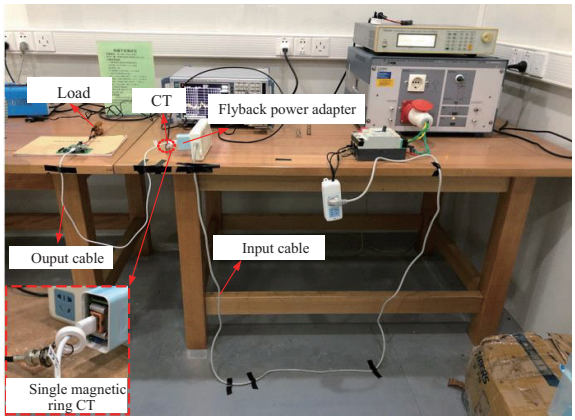

Fig. 20. CM current test setup diagram (CT).

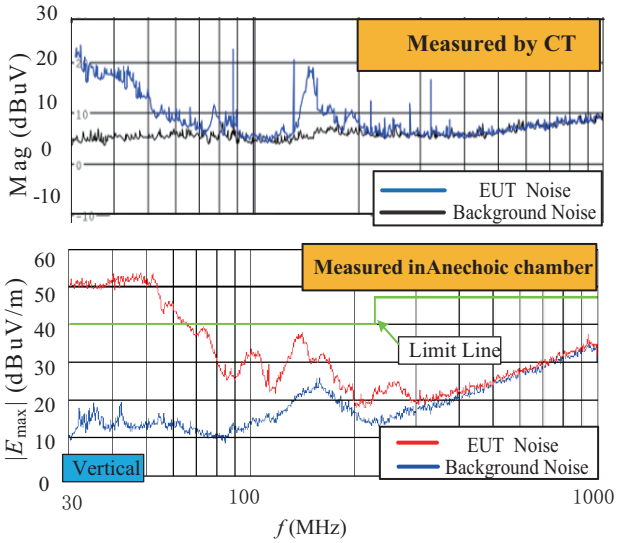

Fig. 21. Comparison of EZ17 measurement results and anechoic chamber measurement results.

A. CT Measures the Common Mode Current

Use the setting of the second part, and use CT to measure the common mode current. The experimental equipment is placed as shown in Fig. 20.

The test result is shown in Fig. 21, and it can be seen that the effective bandwidth of CT is 30~200 MHz, which is better

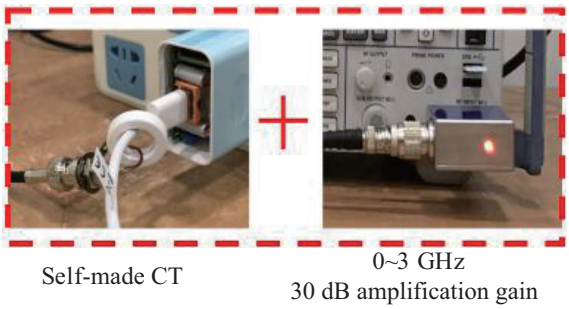

Fig. 22. Single magnetic ring CT with preamplifier.

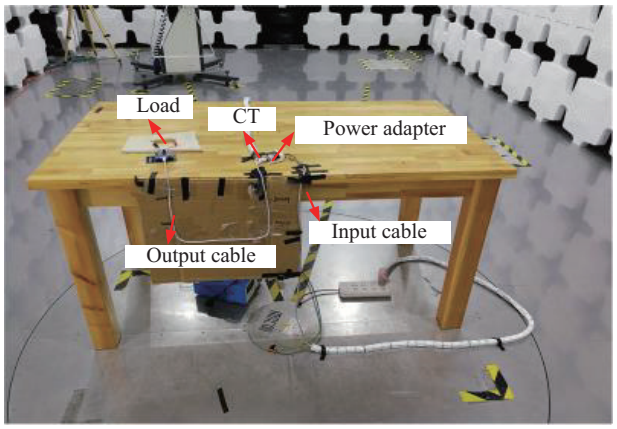

Fig. 23. 3m Semi-Anechoic Chamber CT measurement platform setup.

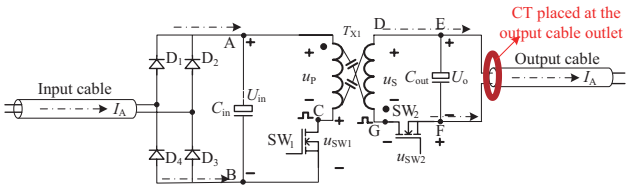

Fig. 24. Circuit schematic and CT placement diagram.

than 30~46 MHz of EZ-17.

B. Comparison of Standard Radiation Measurements and CT Measurement Currents in a Chamber Environment

Due to the low amplitude of the noise of the measured sample, the CT can only measure the common mode current within 30 MHz~200 MHz, so the preamplifier can be added to measure the radiation noise, and the setting is shown in Fig. 22.

In order to verify the validity of the designed CT to measure radiation, the radiation test results of two different cases are used to compare with the self-made CT test results.

The measurement platform in the 3m chamber is set up as shown in Fig. 23, and the self-made CT should be placed at the exit of the output cable.

Case 1: Circuit principle and CT placement are shown in Fig. 24. In the semi-anechoic chamber, CT measurement results and the antenna received radiation results of the comparison as Fig. 25, can be seen in the 30 MHz~200 MHz band,

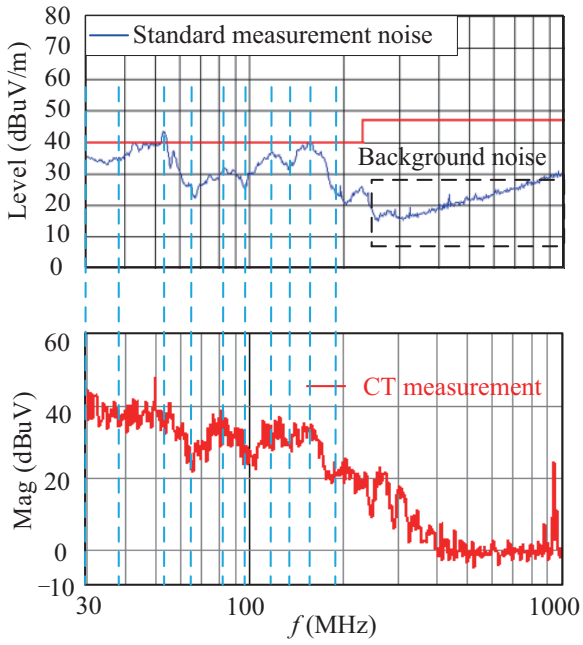

Fig. 25. Comparison of anechoic chamber measurement results and CT measurement results.

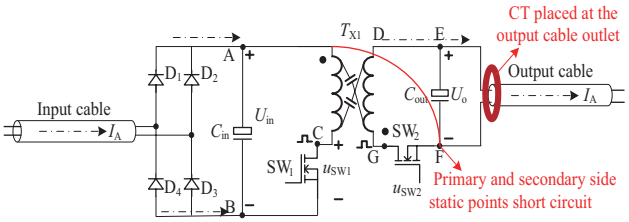

Fig. 26. Transformer static point shorting circuit schematic.

CT measurement common mode noise current results and the antenna measurement field strength of the vertical component trend consistency is good, above 200 MHz are the background noise. The results not only verify the common mode noise current is the main factor of the converter to generate radiation EMI but also verify the validity of the self-made CT measurement radiation EMI trend.

Case 2: The transformer primary and secondary static points are connected, and the circuit principle is shown in Fig. 26. Fig. 27 shows the comparison between the CT measurement results and the antenna received radiation results in the 3m semi-anechoic chamber. It can be seen that in the 30 MHz~200 MHz band, the CT measurement common mode noise current results and the antenna measurement vertical component trend consistency is good, above 200 MHz is the background noise. This result also verifies the correctness of the proposed theory and the validity of the self-made CT measurement. It is worth mentioning that the spike near 1 GHz in the CT measurement result is caused by the background noise of the receiver.

As shown in Fig. 28, because the noise above 200 MHz is covered by background noise, no comparison is meaningful, so take the effective frequency point of 30 MHz~200 MHz comparison. At 100 MHz, the standard measurement is down about

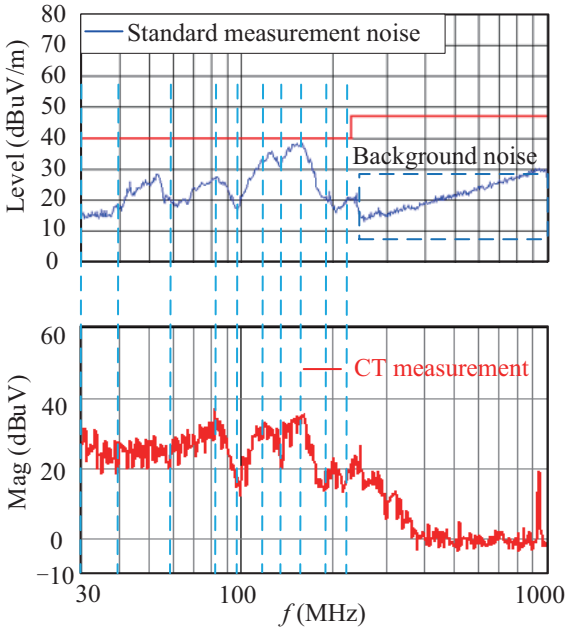

Fig. 27. Comparison of anechoic chamber measurement results and CT measurement results (static point shorting).

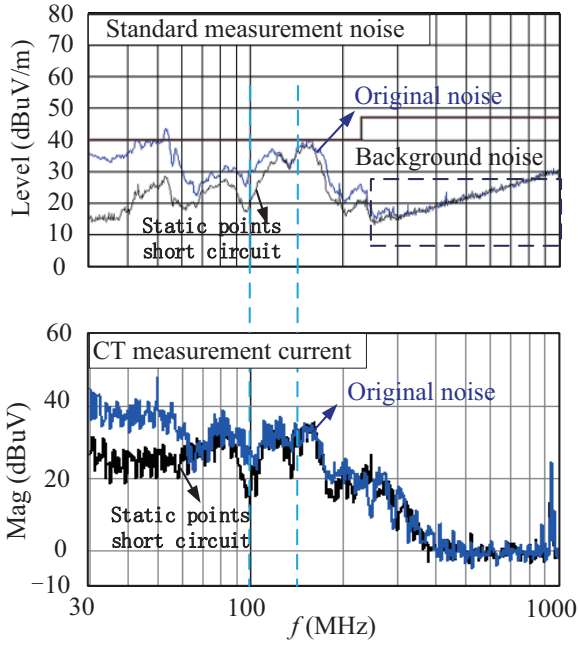

Fig. 28. Comparison of anechoic chamber measurement results and CT measurement results for different cases.

10 dB, CT measurement is down about 8 dB; at 160 MHz, the standard is down about 0 dB, CT measurement is down about 0 dB. Two sets of experiments verified that the common mode noise current measured by CT is proportional to the maximum electric field strength obtained from the standard measurement of radiation EMI.

This verifies the validity of the CT measurements, so we can use the common mode currents measured by CT to determine the strength of the radiated EMI.

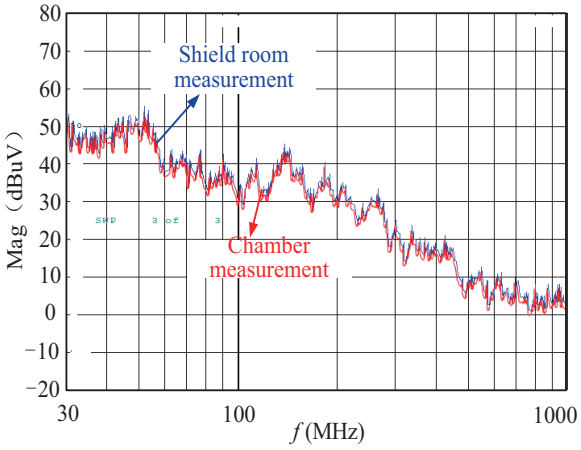

Fig. 29. Comparison of measurement results of CT in shielded room and chamber.

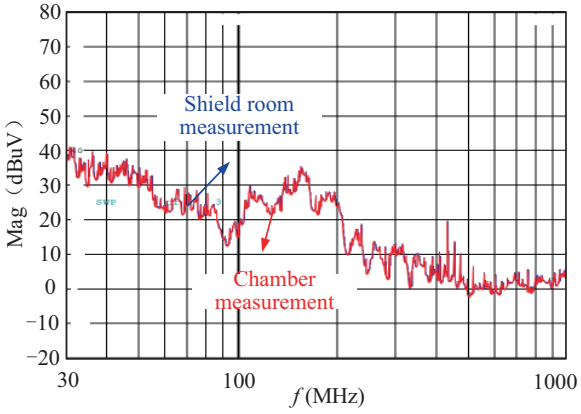

Fig. 30. Comparison of measurement results of CT in shielded room and chamber.

C. Test Environment on CT Measurement Radiation EMI Impact Analysis

The chamber is expensive, and most laboratories can't be equipped with a chamber. Even if some universities and companies are equipped with a chamber environment, the use of resources is very tight, so if the radiation EMI level can be evaluated not in a chamber environment, not only reduces the measurement cost but also solves the pressure of resource constraints.

The first set of measurements is set as an ordinary flyback power supply without filtering devices, that is, without a common mode inductor and without a Y capacitor. Under this situation, the measurement results of CT in the chamber and the measurement results of CT in the chamber are compared as shown in Fig. 29, and the results show that the consistency of the measurement in the chamber environment and the measurement results in the shielding room is good.

The second set of measurements is set as an ordinary flyback power supply with filtering devices, that is, with a common mode inductor and Y capacitor. Under this situation, the measurement results of CT in the chamber and the measurement results of CT in the shielding room are compared as shown in Fig. 30 and the results show that the consistency of the mea-

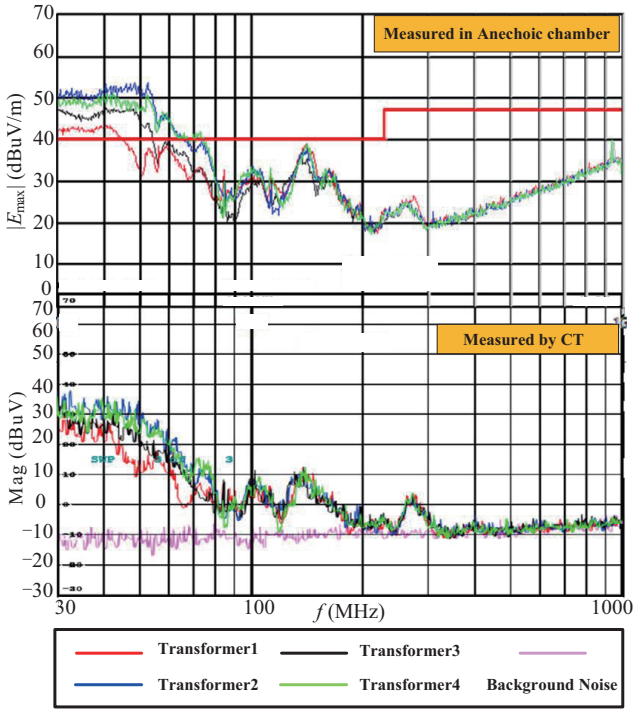

Fig. 31. Comparison of anechoic chamber measurement results and CT measurement results for different transformers.

surement in the chamber environment and the measurement results in the shielding room is very good.

D. Comparison of Measurement Results for the Prototype Using Different Transformers

Replacing the transformer on this prototype, theoretically speaking, for the same prototype with different transformers, there will be differences in the noise level generated. Choosing four different transformers of the same scheme, theoretically, the noise of these four transformers will be different, but the overall trend should be consistent.

The upper part of Fig. 31 shows the standard radiation measurement and the lower part shows the measurement results using CT in the shielding room.

We compare the standard measurement results in the anechoic chamber with the results measured by CT in the shielding room, and it can be found that CT can measure the subtle differences of different noises and has good consistency with the standard measurement results in the anechoic chamber, which is also in line with the previous experimental results.

VII. Conclusion

(1) Based on the mechanism that the magnitude of radiated EMI is directly proportional to the common-mode current, we propose a method that can use CTs to evaluate the strength of radiation and then optimize the design of current transformers based on the principle of electromagnetic fields and the influence of material frequency characteristics.

(2) By comparing CT measurements of radiated EMI in both anechoic chamber and shielded room environments, we demonstrate the applicability of our proposed method in non-chamber settings for evaluating radiated EMI trends. This comparison underscores the versatility of the CT-based approach in diverse environmental conditions.

(3) The correlation between standard radiation measurements in chamber environments and CT-measured currents in non-chamber settings substantiates the accuracy of our custom CT in assessing radiation EMI strength. This comparison not only validates our CT measurement technique but also serves as a technical reference for analyzing and evaluating the factors influencing radiated electromagnetic interference.

References

[1] H. Zhang, S. Wang, Y. Li, Q. Wang, and D. Fu, "Two-capacitor transformer winding capacitance models for common-mode EMI noise analysis in isolated DC–DC converters," in *IEEE Transactions on Power Electronics*, vol. 32, no. 11, pp. 8458–8469, Nov. 2017.

[2] Z. Lu and W. Chen, "Common mode EMI noise reduction technique by noise path configuration of high frequency power transformer," in *2009 IEEE 6th International Power Electronics and Motion Control Conference*, Wuhan, China, 2009, pp. 954–956.

[3] Y. P. Chan, B. M. H. Pong, N. K. Poon, and J. C. P. Liu, "Common-mode noise cancellation by an antiphase winding in multilayer isolated planar transformer," in *IEEE Transactions on Electromagnetic Compatibility*, vol. 56, no. 1, pp. 67–73, Feb. 2014.

[4] L. Xie, X. Ruan, and Z. Ye, "Equivalent noise source: An effective method for analyzing common-mode noise in isolated power converters," in *IEEE Transactions on Industrial Electronics*, vol. 63, no. 5, pp. 2913–2924, May 2016.

[5] H. Chen, Z. Zheng, and J. Xiao, "Determining the number of transformer shielding winding turns for suppressing common-mode noise in flyback converters," in *IEEE Transactions on Electromagnetic Compatibility*, vol. 60, no. 5, pp. 1606–1609, Oct. 2018.

[6] L. Xie, X. Ruan, Q. Ji, and Z. Ye, "Shielding-cancelation technique for suppressing common-mode EMI in isolated power converters," in *IEEE Transactions on Industrial Electronics*, vol. 62, no. 5, pp. 2814–2822, May 2015.

[7] C. R. Paul, "A comparison of the contributions of common-mode and differential-mode currents in radiated emissions," in *IEEE Transactions on Electromagnetic Compatibility*, vol. 31, no. 2, pp. 189–193, May 1989.

[8] J. Yao, Y. Li, H. Zhao, S. Wang, Y. Lu, and D. Fu, "Modeling and reduction of radiated common mode current in flyback converters," in *2018 IEEE Energy Conversion Congress and Exposition (ECCE)*, Portland, OR, USA, 2018, pp. 6613–6620.

[9] W. Meng, F. Zhang, Z. Fu, and G. Dong, "High dv/dt noise modeling and reduction on control circuits of GaN-based full bridge inverters," in *IEEE Transactions on Power Electronics*, vol. 34, no. 12, pp. 12246–12261, Dec. 2019.

[10] J. Yao, Y. Li, S. Wang, X. Huang, and X. Lyu, "Analysis and reduction of radiated EMI in high-frequency GaN IC-based active clamp flyback converters," in *2020 IEEE Applied Power Electronics Conference and Exposition (APEC)*, New Orleans, LA, USA, 2020, pp. 664–671.

[11] J. Yao, Y. Li, H. Zhao, and S. Wang, "Design of CM inductor based on core loss for radiated EMI reduction in power converters," in *2019 IEEE Applied Power Electronics Conference and Exposition (APEC)*, Anaheim, CA, USA, 2019, pp. 2673–2680.

[12] Y. Li, H. Zhang, S. Wang, H. Sheng, C. P. Chng, and S. Lakshmikanthan, "Investigating switching transformers for common mode EMI reduction to remove common mode EMI filters and Y-capacitors in flyback converters," in *IEEE Journal of Emerging and Selected Topics in Power Electronics*, vol. 6, no. 4, pp. 2287–2301, Dec. 2018.

[13] W. Padungtin and V. Tarateeraseth, "A study of radiated EMI predictions from measured common-mode currents for switching power supplies," in *2020 17th International Conference on Electrical Engineering/*

Electronics, Computer, Telecommunications and Information Technology (ECTI-CON), Phuket, Thailand, 2020, pp. 76–79.

[14] Y. Zhang, S. Wang, and Y. Chu, "Modeling and reduction of radiated EMI for isolated power converters," in *2018 IEEE Applied Power Electronics Conference and Exposition (APEC)*, San Antonio, TX, USA, 2018, pp. 1778–1785.

[15] C. R. Paul and D. R. Bush, "Radiated emissions from common-mode currents," in *1987 IEEE International Symposium on Electromagnetic Compatibility*, Atlanta, GA, USA, 1987, pp. 1–7.

[16] Y. Zhang, S. Wang, and Y. Chu, "Comparison of radiated electromagnetic interference (EMI) generated by power converters with silicon MOSFETs and GaN HEMTs," in *2019 IEEE Applied Power Electronics Conference and Exposition (APEC)*, Anaheim, CA, USA, 2019, pp. 1375–1382.

[17] J. Yao, S. Wang, and H. Zhao, "Measurement techniques of common mode currents, voltages, and impedances in a flyback converter for radiated EMI diagnosis," in *IEEE Transactions on Electromagnetic Compatibility*, vol. 61, no. 6, pp. 1997–2005, Dec. 2019.

[18] W. Kenneth, "The HF current probe: theory and application." in *Interference Technology: EMC Directory & Design Guide 2012*, 2012, pp. 1–6.

[19] O. Väänänen, "Do-it-yourself current probe characterization for EMC troubleshooting," in *2014 International Symposium on Fundamentals of Electrical Engineering (ISFEE)*, Bucharest, Romania, 2014, pp. 1–4.

Qingbin Chen was born in Quanzhou, China. He received the B.E. and Ph.D. degrees in electrical engineering from Fuzhou University, Fuzhou, China in 2007 and 2012, respectively. He worked as a visiting scholar in University of Florida, Florida, the USA from 2017 to 2018. His research includes high frequency magnetic technology, EMC diagnosis and suppression technology, wireless power transfer. Dr. Chen is the member of Magnetic Components and Ferrite Materials (Magnetic Standards Committee of China) and served as the Vice chairperson and Deputy Secretary General of Magnetic Component Specialty Committee of CPSS (China Power Supply Society).

Qinwen Yang was born in Shanxi, China, in 1999. He received the B.S. degree in Electrical engineering and automation from the Fuzhou University of Science and Technology, China, in 2021. He is currently pursuing the master's degree with the Fuzhou University, Fuzhou. His research interest includes high frequency magnetic technology.

Jianxin Shi was born in Huzhou, China, in 1995. He received the B.S. degree in Electrical engineering and automation from College of Science & Technology Ningbo University, China, in 2018. He received the master's degree in Electrical Engineering and Automation from the Fuzhou University, Fuzhou, China, in 2023. His research interest includes high frequency magnetic technology.

Shaohui Xu was born in Quanzhou, China, in 1996. He received the B.S. degree in Electrical Engineering and Automation from the Fuzhou University, China, in 2019. He received the master's degree in Electrical Engineering and Automation from the Fuzhou University, Fuzhou, China, in 2022. His research interest includes high frequency magnetic technology.